Çanakkale Onsekiz Mart University

Journal of Advanced Research in Natural and Applied Sciences

dergipark.org.tr/tr/pub/jarnas

Open Access

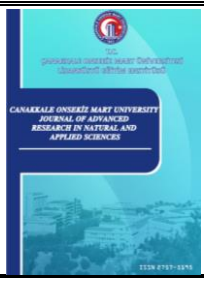

e-ISSN: 2757-5195 2024, Vol. 10, Issue 3, Pages: 669-683 doi.org/10.28979/jarnas.1495889

Multi-Focus Image Fusion Using Energy Valley Optimization Algorithm

Harun Akbulut[1]

[1]Department of Computer Engineering, Faculty of Engineering and Architecture, Nevşehir Hacı Bektaş Veli University, Nevşehir, Türkiye

Article Info
Received: 04 Jun 2024
Accepted: 25 Jul 2024
Published: 30 Sep 2024
Research Article

Abstract − When a natural scene is photographed using imaging sensors commonly used today, part of the image is obtained sharply while the other part is obtained blurry. This problem is called limited depth of field. This problem can be solved by fusing the sharper parts of multi-focus images of the same scene. These methods are called multi-focus image fusion methods. This study proposes a block-based multi-focus image fusion method using the Energy Valley Optimization Algorithm (EVOA), which has been introduced in recent years. In the proposed method, the source images are first divided into uniform blocks, and then the sharper blocks are determined using the criterion function. By fusing these blocks, a fused image is obtained. EVOA is used to optimize the block size. The function that maximizes the quality of the fused image is used as the fitness function of the EVOA. The proposed method has been applied to commonly used image sets. The obtained experimental results are compared with the well-known Genetic Algorithm (GA), Differential Evolution Algorithm (DE), and Artificial Bee Colony Optimization Algorithm (ABC). The experimental results show that EVOA can compete with the other block-based multi-focus image fusion algorithms.

Keywords − *Multi-focus image fusion, energy valley optimizer, block-based image fusion, comparison of meta-heuristic algorithms*

1. Introduction

Image fusion methods have recently become more useful in human perception and computer vision applications. Image fusion can obtain a single image containing more information from multiple images of the same scene. These images of the same scene can be obtained from a single sensor whose perceptual parameters can be changed or from different sensors. The first method is called single-sensor image fusion, while the other is called multi-sensor image fusion. The fused images are used more efficiently in many fields, from health to military fields [1-3].

Imaging sensors commonly used today cannot display the entire natural scene. Sensors focus on an object in the natural scene and photograph the focused area. The area outside the focus area is displayed as blurry. Due to these limitations of the sensors, some of the obtained images are clear, while the other parts are blurred. This problem can be solved by combining clear parts of multi-focus images of the same scene. These methods are called multi-focus image fusion (MFIF). MFIF methods can be examined in four groups: transformation domain, spatial domain, deep learning, and hybrid-based methods [4].

In transformation-based methods, the source images are first transferred to the transformation space using a transformation algorithm. Then, by applying the fusion rule, the source images are combined in the

[1]harun.akbulut@nevsehir.edu.tr (Corresponding Author)

transformation space. Then, the fused image is obtained by applying the inverse transformation process. Transform-based multi-focus image fusion methods have been presented using many transformation algorithms such as discrete wavelet transform [5], Laplacian transform [6], Curvelet transform [7], Contourlet transform [8], and Shearlet transform [9]. In these methods, artificial images may appear in the fused image because any possible error in the transformation space will be reflected in the entire image. In addition, transformation and reverse transformation processes take a long time. These problems are seen as disadvantages of transformation-based methods.

Another method for MFIF is spatial-based methods. These methods can be examined in two parts: pixel and region based. Pixel-based methods aim to transfer sharp pixels in the source images to the fused image [10]. The sharpness function used in this method for selecting sharp pixels is important. The sharpening criterion function directly affects the method's performance [11]. This method provides more effective results than the transformation-based method because the sharp pixels in the source images are directly transferred to the fused image. However, since this method only deals with the pixel's attribute and not the neighboring pixel values around it, undesirable situations may arise in the fused image. In addition, this method will take a longer calculation time since all pixel values will be processed separately [12].

Due to the above-mentioned disadvantage of the pixel-based method, region-based MFIF methods have been proposed. The basic idea of these methods is to move sharper pixel groups to the fused image by taking advantage of the sharpness information of both a pixel and the relevant pixel and neighboring pixels. Region-based methods have less computational cost, and the obtained results are more satisfactory because they also consider neighboring pixel values. The first block-based multi-focal image fusion method is proposed by Li et al. [13]. The proposed method first divides the source images into identical blocks. Then, the sharper blocks are identified using the spatial frequency criterion function and moved into the merged image. Another method that is based on combining the focus maps obtained by block-based focus measures and employing a multi-matting model with weight maps is proposed by Chen et al. [14]. Based on the optimal placing of the blocks multi-focal method is proposed by Toprak and Aslantaş [15]. Using a differential evolution algorithm based on point distribution functions of source images multi-focus image fusion method is presented by Aslantaş and Toprak [16]. Using a genetic algorithm, multi-focus image fusion is presented by Kong et al. [17]. Aslantas and Kurban suggest a multi-focus method based on optimizing block size using a differential evolution algorithm [1].

Despite numerous studies on multi-focus image fusion in the literature, there remains a critical need for enhancing the quality of fused images obtained. Particularly noteworthy is the recent utilization of artificial intelligence techniques that have effectively solved various non-linear problems [18, 19]. Therefore, evaluating current problems with recently proposed artificial intelligence techniques is crucial. This article proposes a method using Energy Valley Optimization Algorithm (EVOA) for block-based multi-focus image fusion. EVOA is used to optimize the block size of the source images. For the fitness function of EVOA, the function that maximizes the variance value of the fused image is used. The method is applied to commonly used test data sets. The objective and subjective evaluation results show that EVOA provides satisfactory results for multi-focal image fusion. EVOA has demonstrated that it can compete with commonly used meta-heuristic algorithms such as Genetic Algorithm (GA), Evolution Algorithm (DE), and Artificial Bee Colony Optimization Algorithm (ABC). The contribution of the study is as follows:

i. In this study, EVOA is used for multi-focus image fusion for the first time,

ii. The proposed method is applied to commonly used datasets,

iii. The obtained fused images are evaluated with quality metrics to obtain numerical results,

iv. Numerical results are compared with a well-known meta-heuristic optimization algorithm: GA, DE, and ABC.

In the remaining part of our study, the proposed method and quality metrics are mentioned in the second part, the Energy Valley Optimization Algorithm. In the third section, the results of the conducted experiments are given. Finally, the results and discussion section are provided.

2. Block-based Multi-focus Image Fusion Using Energy Valley Optimization Algorithm

2.1. Energy Valley Optimization Algorithm

EVOA is a meta-heuristic optimization algorithm proposed by Azizi et al. [18] in 2023. EVOA aims to solve optimization problems inspired by advanced physics principles. In this context, meta-heuristic algorithms belong to the class of physics-based meta-heuristic optimization algorithms. EVOA mimics the degradation process caused by different particles in nature. In EVOA, each particle with varying levels of stability represents a possible solution. The algorithm first starts with the creation of the initial population. The initial population is created using (2.1).

$$x_i^j = x_{i,min}^j + rand \cdot \left(x_{i,max}^j - x_{i,min}^j\right), \quad i \in \{1,2,3,\cdots,n\} \text{ and } j \in \{1,2,3,\cdots,d\} \tag{2.1}$$

Here, n refers to the number of pieces in the solution space, and d refers to the problem size. $x_{i,min}^j$ and $x_{i,max}^j$ represent the lower and upper bounds of the problem, respectively. The second step calculates the neutron enrichment level using (2.2).

$$EB = \frac{\sum_{i=1}^{n} NEL_i}{n}, \quad i \in \{1,2,3,\cdots,n\} \tag{2.2}$$

Here, NEL_i *i-th* represents the neutron enrichment level of the particle, and EB refers to the enrichment limit of the particles. The stability levels of the particles are calculated using (2.3).

$$SL_i = \frac{NEL_i - BS}{WS - BS}, \quad i \in \{1,2,3,\cdots,n\} \tag{2.3}$$

Here, SL_i *i-th*. *BS* and *WS* represent the stability level of the particle, and *BS* and *WS* represent the best and worst particle stability levels, respectively. In EVOA, a new particle is generated using (2.4).

$$x_i^{New1} = x_i\left(x_{BS}\left(x_i^j\right)\right), \quad i \in \{1,2,3,\cdots,n\} \text{ and } j = Alpha\ Index\ II \tag{2.4}$$

Here, x_i^{New1} represents the newly produced particle, x_i represents the position of the current particle and x_{BS} represents the best particle in the solution space. Particles in the universe interact with each other by emitting rays. Accordingly, the second new individual is created using (2.5) based on neighbor interaction.

$$x_i^{New2} = x_i\left(x_{NG}\left(x_i^j\right)\right), \quad i \in \{1,2,3,\cdots,n\} \text{ and } j = Gamma\ Index\ II \tag{2.5}$$

Here, x_i^{New2} represents the newly produced particle and x_{NG} represents the neighboring particles that emit photons. If the stability level of a particle is lower than the stability limit, its degradation is considered to have occurred. Thus, the stability level of these particles is updated to the particle with the best stability level and to the center of the particles using (2.6).

$$x_i^{New1} = x_i + \frac{\left(r_1 x_{BS} - r_2 \frac{\sum_{i=1}^{n} x_i}{n}\right)}{SL_i}, \quad i \in \{1,2,3,\cdots,n\} \tag{2.6}$$

Here, $r_1, r_2 \in [0,1]$ and SL_i represents the stability level of the particle in the *i-th* iteration. To increase the exploration and exploitation speed of the algorithm, a location update is performed using (2.7).

$$x_i^{New2} = x_i + (r_3 \cdot x_{BS} - r_4 \cdot x_{NG}), \quad i \in \{1,2,3,\cdots,n\} \tag{2.7}$$

Here, $r_3, r_4 \in [0,1]$ and x_{NG}denote the stability level of the neighboring particle. If the stability level of a particle is less than the neutron enrichment limit, the position update is performed randomly using (2.8).

$$x_i^{New} = x_i + r, \quad i \in \{1,2,3,\cdots,n\} \tag{2.8}$$

Here, $r \in [0,1]$, x_i denotes the current position and x_i^{New} denotes the new position. Position updates of the particles are made throughout the algorithm's main loop. Thus, it is aimed to reach the best solution. The basic steps of EVOA are shown in Figure 1.

2.2. Block-based Multi-focus Image Fusion Using Energy Valley Optimization Algorithm

In block-based MFIF methods, the source images are first divided into $m \times n$-sized blocks. Then, using the sharpness criterion function, sharper blocks are detected and moved to the fused image to obtain the fused image. Since each image will have its attributes, a block method with a fixed $m \times n$ size will not give good results for every image. Thus, the $m \times n$ block size must be determined by researchers for each image. The determined block size will directly affect the performance of the method. Optimization algorithms can be used effectively to compute the optimal block size. The flow chart of the optimized block-based method is shown in Figure 2 [4].

As shown in Figure 2, the source images are first divided into $m \times n$ -sized blocks. The optimization algorithm starts the cycle with random $m \times n$ block size generation. During each cycle, blocks with $m \times n$ block size are compared using the sharpness criterion function. Blocks with greater sharpness criterion function are transferred to the fused image. This study uses the spatial frequency (SF) [19] criterion function as the sharpness criterion function. SF is a criterion function that measures overall activity in the image by highlighting differences between neighboring pixels. The sharpness value of each block is calculated using (2.9)-(2.11).

$$SF = \sqrt{R^2 + C^2} \tag{2.9}$$

$$R = \sqrt{\frac{1}{mxn}\sum_i \sum_j [f(i,j) - f(i-1,j)]^2} \tag{2.10}$$

$$C = \sqrt{\frac{1}{mxn}\sum_i \sum_j [f(i,j) - f(i,j-1)]^2} \tag{2.11}$$

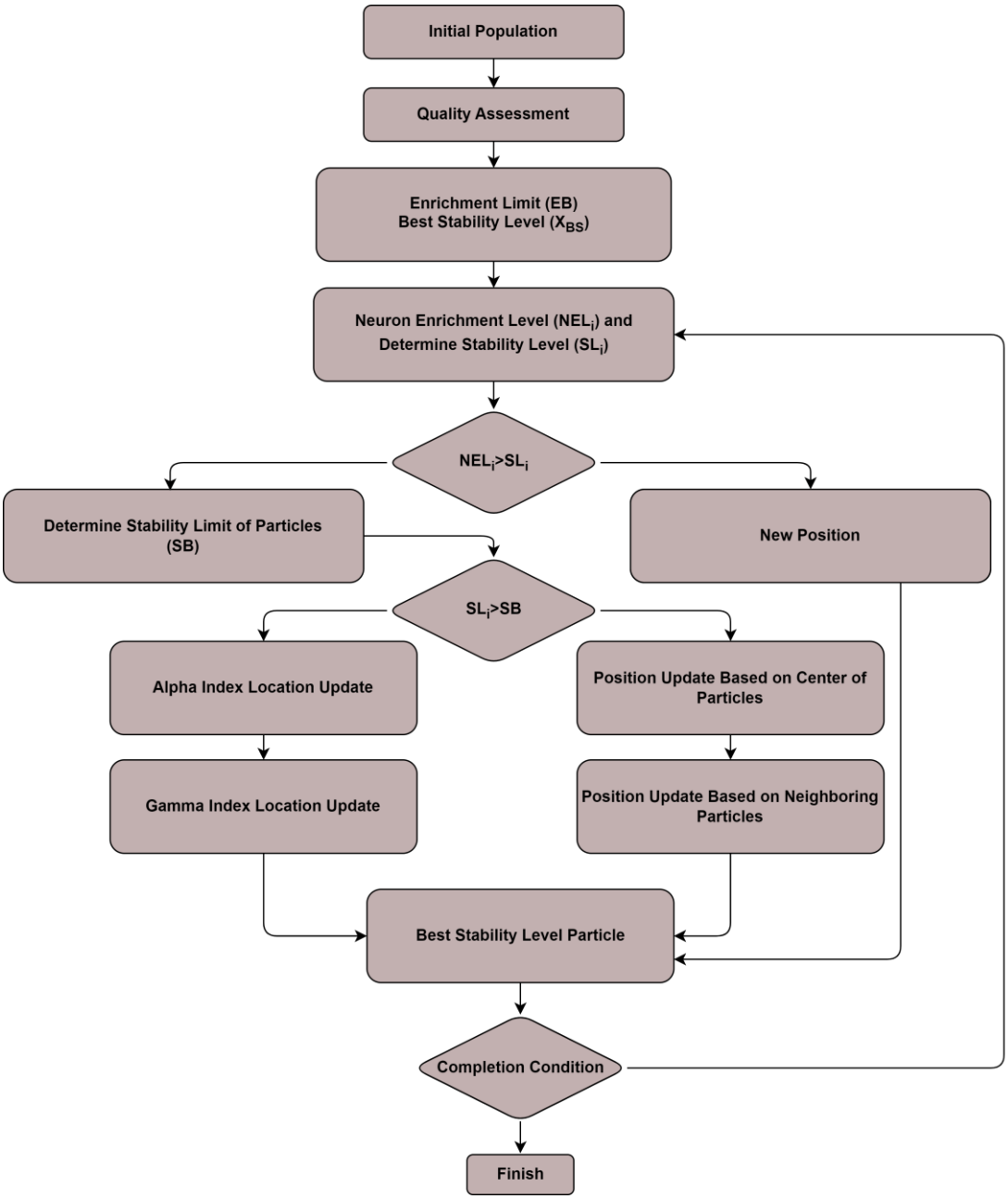

Figure 1. EVOA flowchart

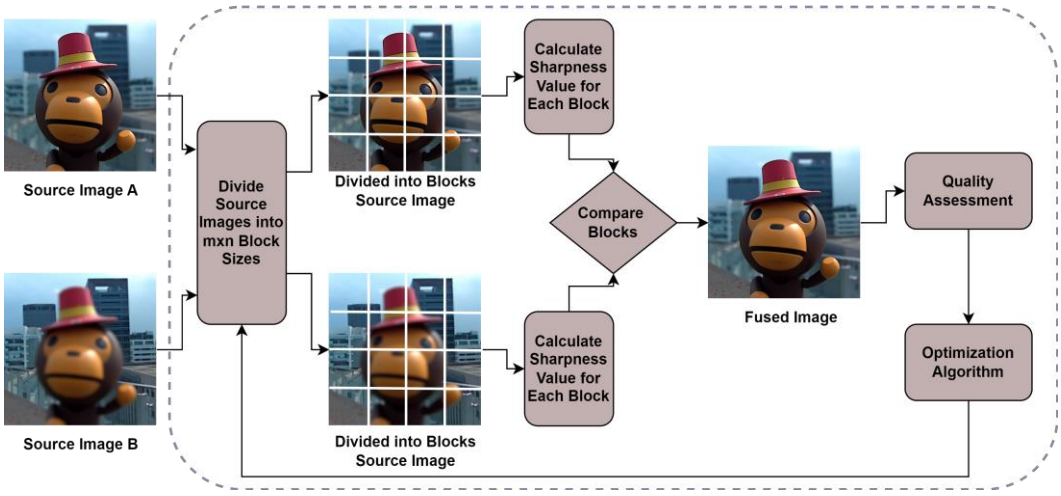

Figure 2. Multi-focus image fusion flowchart by optimization algorithm

Blocks with higher SF values are moved to the fused image. F represents the fused image, and Cr represents the criterion function. Sharper blocks are selected using (2.12) and moved to the fused image.

$$F_i = \begin{cases} A_i, & Cr_i^A \geq Cr_i^B \\ B_i, & \text{otherwise} \end{cases} \tag{2.12}$$

Then, the fused image is obtained. The quality of the fused image is evaluated using the variance (QM_{Var}) [22] quality metric. The QM_{Var} value of the fused image is calculated using (2.13), where μ is the average value of the F and $m \times n$ is the size of the F.

$$\mathrm{QM}_{Var}(F) = \frac{1}{m \times n} \sum_{(i,j)} (F(i,j) - \mu)^2 \tag{2.13}$$

The function that maximizes the variance value of the fused image is used as the fitness function of the optimization algorithm. In this study, EVOA, proposed in recent years, is used as the optimization algorithm.

2.3. Compared Optimization Algorithms

Information about the metaheuristic optimization algorithms that are GA, DE, and ABC is provided in this section. These well-known, widely used, and meta-heuristic optimization algorithms give good results in optimization problems. GA belongs to the evolutionary, DE numerical, and ABC belongs to the intelligent swarm metaheuristic class of optimization algorithms. Thus, EVOA is compared with algorithms representative of many classes of metaheuristic optimization algorithms.

2.3.1. Genetic Algorithm (GA)

GA [23] is a population-based optimization algorithm developed by Holland and colleagues in 1975, widely used for solving multidimensional and non-linear problems, and known for delivering effective results. GA solves optimization problems by employing genetic operators such as selection, crossover, and mutation. The selection genetic operator ensures the survival of individuals with high solution quality during the algorithm's iterations while gradually eliminating individuals with low solution quality. The crossover genetic operator aims to produce higher-quality individuals by combining pairs of randomly selected individuals from the solution pool. The mutation genetic operator seeks to generate new individuals from randomly selected ones in the solution pool to create individuals with potentially better solution quality.

2.3.2. Differential Evolution Algorithm (DE)

DE [24] is a stochastic, population-based metaheuristic algorithm introduced by Storn and Price, known for being fast and stable and delivering effective results in optimizing multidimensional and non-linear problems, especially in numerical optimization. Since DE is a stochastic evolution algorithm, it generates the initial population randomly. DE employs a unique mutation method that creates a new individual by adding the weighted difference of two randomly selected individuals from the solution pool, determined by a parameter F specified by the researcher, to the value of a third individual.

2.3.3. Artificial Bee Colony Optimization Algorithm (ABC)

ABC algorithm [25], developed by Karaboga and Basturk, is a recent optimization algorithm based on swarm intelligence that models the intelligent foraging behavior of honeybees for numerical optimization problems. The ABC algorithm mathematically models the aforementioned intelligent behaviors of honeybee colonies in nature, yielding effective results in solving numerical optimization problems. In the ABC algorithm, food source regions represent potential solution values for the problem to be solved. Once scout bees detect food

sources, employed bees are sent to these sources. Employed bees evaluate the quality of the food sources they work on and the neighboring sources, gravitating towards the source with better solution quality. When an employed bee with a current solution and new location information returns to the hive, it communicates this information to the onlooker bees through a dance. When the food quantity is depleted, reaching the threshold specified by the limit parameter of the ABC algorithm, the employed bee becomes a scout bee and continues searching again.

2.4. Quality Metrics

In image fusion, quality metrics play a crucial role in evaluating the effectiveness of the fusion process, which aims to integrate information from multiple images into a single fused image with improved visual quality and information content. These metrics provide quantitative measures to assess various aspects such as spatial resolution, spectral fidelity, contrast, and overall perceptual quality of the fused image. However, a single quality metric that considers all images' quality has not yet been developed. Therefore, it is necessary to evaluate the quality of an image using multiple quality metrics. This section includes a variety of quality metrics for the objective assessment of fused images. These metrics have been selected from commonly used quality metrics in image fusion. Variance (QM_{Var}) and Spatial Frequency (QM_{SF}) are mentioned in (2.13) and (2.9)-(2.11), respectively.

2.4.1. Entropy (QM_E)

Entropy [26] is a quality metric that measures the content information of a fused image. As the entropy value increases, the quality of the fused image increases. Entropy is calculated using (2.14).

$$\mathrm{QM}_E(F) = -\sum_{i=0}^{L} h_f(i)\log_2 h_f(i) \tag{2.14}$$

Here, L is the number of gray tones, h_f is the normalized histogram of the fused image.

2.4.2. Standard Deviation (QM_{SD})

Standard deviation [27] is a quality metric measuring the fused image's contrast. As the QM_{SD} value increases, the quality of the fused image increases. QM_{SD} is calculated using (2.15).

$$\mathrm{QM}_{SD}(F) = \sqrt{\sum_{i=0}^{L} (i-\bar{\imath})^2 \log_2 h_f(i)} \tag{2.15}$$

Here, L is the number of gray tones, h_f is the normalized histogram of the fused image.

2.4.3. Edge Based Quality Metric (QM_{ABF})

QM_{ABF} [28] is a quality metric that calculates the quality of the image by using edge information. QM_{ABF} is computed using (2.16).

$$\mathrm{QM}_{ABF}(F) = \frac{\sum_{n=1}^{N}\sum_{m=1}^{M} Q^{AF}(n,m)w^{A}(n,m) + Q^{BF}(n,m)w^{B}(n,m)}{\sum_{n=1}^{N}\sum_{m=1}^{M}(w^{A}(n,m) + w^{B}(n,m))} \tag{2.16}$$

Here, $Q^{A/BF}$ denotes weighted by $w^{A/B}(n,m)$.

2.4.4. Chen-Blum Metric (QM_{CB})

QM_{CB} [29] is a quality metric that calculates the quality of the image using a saliency map. As the QM_{CB} value increases, the quality of the image increases. QM_{CB} is calculated using (2.17).

$$\mathrm{QM}_{CB}(F) = Sm_A(x,y)Q_{AF}(x,y) + Sm_B(x,y)Q_{BF}(x,y) \tag{2.17}$$

Here, $Sm_A(x,y)$ denotes a global quality map.

2.4.5. Mutual Information (QM_{MI})

QM_{MI} [30] is a quality metric measuring the similarity information between the fused and the source images. QM_{MI} is calculated using (2.18).

$$\mathrm{QM}_{MI}(F) = \sum_{i=1}^{L}\sum_{j=1}^{L} h_{sf}(i,j)\log_2 \frac{h_{sf}(i,j)}{h_s(i,j)h_f(i,j)} \tag{2.18}$$

Here, h_s and h_f denotes the normalized histogram of the source and fused image, respectively. L represents the number of gray tones.

2.4.6. Sum of the Correlations of Differences (QM_{SCD})

QM_{SCD} [31] is a quality metric that determines the quality of the image according to the correlation coefficient between the fused image and the different images. SCD is calculated using (2.19).

$$\mathrm{QM}_{SCD}(F) = c(D_A,F) + c(D_B,F) \tag{2.19}$$

Here, c denotes the correlation coefficient, $D_{A/F}$ denote the different images.

3. Experimental Results

This study proposes a method based on block size optimization for multi-focus image fusion using EVOA. Several experiments are conducted to test the performance of the method. The experiments use a laptop with Windows 7 operating system, 8 GB RAM, Intel Core 2.3 features and MATLAB r2019a. Experiments are carried out on the 512x512 color Lytro dataset. EVOA has been run independently thirty times. Max, mean, and standard deviation values of experiments are obtained. Numerical results are obtained using the eight quality functions used for image quality evaluation in the literature. Figure 3 shows test images taken from the Lytro [10] dataset where the experiments are carried out. To ensure fairness, common parameter values for optimization algorithms, namely a population size of 10 and a maximum iteration count of 100, have been selected. These values were chosen based on insights from the literature and preliminary experiments conducted.

The parameter values used for GA, DE, and ABC are those commonly used in the literature and generally observed to yield good results. For GA, the selection strategy is roulette wheel selection, with single-point crossover and a crossover rate of 0.8. The mutation strategy is a uniform mutation with a mutation rate of 0.2. A crossover rate of 0.6 and an F value of 0.9 were chosen for DE. The number of onlooker bees equals the population size for ABC, and the L parameter value is set to 100. EVOA does not have its unique control parameter.

In Tables 1-4, the obtained numerical results in the experiments carried out using optimization algorithms are given comparatively. Max, mean, and standard deviation quality metric values are obtained for each

optimization algorithm. QM_{Var}, QM_E, QM_{SF}, QM_{SD}, QM_{ABF}, QM_{CB}, QM_{MI}, and QM_{SCD} in each column, respectively, is given.

Table 1 shows the numerical results of the experiments conducted for the 1st image. When Table 1 is examined, it is seen that GA and EVOA achieve the best value in a single quality metric for the 1st image. It can be said that while DE gives the best results in four quality metrics, ABC provides the best in three. As a result, it can be said that ABC achieved the best result for the first image, followed by DE.

Figure 3. Experimental data sets

Table 1. Experimental results for Image 1

	QM_{Var}	QM_E	QM_{SF}	QM_{SD}	QM_{ABF}	QM_{CB}	QM_{MI}	QM_{SCD}
				GA				
Max	3818,6295	7,5106	7,0564	61,7950	0,7994	0,8627	**0,8564**	0,6483
Mean	3813,7821	7,4613	7,0072	61,2006	0,7951	0,8582	0,8524	0,6436
SD	3,1457	0,0333	0,0337	0,2853	0,0033	0,0036	0,0032	0,0030
				DE				
Max	**3824,0571**	7,5098	7,0659	**61,8389**	**0,8013**	0,8635	0,8561	**0,6554**
Mean	3819,3852	7,4654	7,0214	61,3595	0,7964	0,8582	0,8528	0,6504
SD	3,2401	0,0307	0,0311	0,3212	0,0032	0,0034	0,0025	0,0033
				ABC				
Max	3816,5063	**7,5120**	**7,0891**	61,7778	0,8009	**0,8638**	0,8559	0,6479
Mean	3811,4401	7,4583	7,0402	61,2467	0,7960	0,8591	0,8512	0,6422
SD	2,9729	0,0328	0,0296	0,2614	0,0031	0,0033	0,0032	0,0030
				EVOA				
Max	3818,1955	7,5118	7,0670	61,7915	0,8002	0,8615	0,8559	0,6511
Mean	3812,9763	7,4711	7,0199	61,3342	0,7951	0,8571	0,8516	0,6467
SD	3,1362	0,0285	0,0307	0,3113	0,0034	0,0032	0,0033	0,0029

Boldfaced values indicate the "best" performances.

Table 2 shows the numerical results of the experiments conducted for the second image. When Table 2 is examined, ABC gives the best result in seven quality metrics for the 2nd image. Other algorithms provide the best results in one quality metric. Thus, it can be said that ABC has a superior performance compared to others for this image.

Table 2. Experimental results for Image 2

	QM_{Var}	QM_{E}	QM_{SF}	QM_{SD}	QM_{ABF}	QM_{CB}	QM_{MI}	QM_{SCD}
				GA				
Max	4955,6490	7,5740	5,1673	70,3963	0,7957	0,8539	**0,8926**	0,4765
Mean	4950,7864	7,5258	5,1178	69,9621	0,7907	0,8491	0,8882	0,4718
SD	3,1543	0,0352	0,0271	0,2744	0,0031	0,0032	0,0035	0,0036
				DE				
Max	4959,8559	**7,5755**	5,1695	70,4262	0,7964	0,8530	0,8925	0,4809
Mean	4953,8459	7,5329	5,1117	69,9503	0,7924	0,8486	0,8871	0,4756
SD	2,7059	0,0289	0,0295	0,3262	0,0036	0,0034	0,0033	0,0033
				ABC				
Max	**4965,5762**	7,5753	**5,1939**	**70,4668**	**0,8010**	**0,8541**	0,8925	**0,4816**
Mean	4961,1913	7,5382	5,1572	70,0680	0,7967	0,8494	0,8882	0,4771
SD	2,7592	0,0224	0,0320	0,2814	0,0027	0,0032	0,0033	0,0034
				EVOA				
Max	4959,8559	**7,5755**	5,1695	70,4262	0,7964	0,8530	0,8925	0,4809
Mean	4954,3476	7,5203	5,1260	69,9727	0,7917	0,8482	0,8880	0,4752
SD	3,0449	0,0337	0,0318	0,2889	0,0036	0,0029	0,0037	0,0036

Boldfaced values indicate the "best" performances.

Table 3 shows the numerical results of the experiments conducted for the 3rd image. When Table 3 is examined, DE achieves the best result in six quality metrics for the 3rd image. Then, ABC achieves the best result in two quality metrics, while EVOA achieves the best result in a single quality metric. Thus, it can be said that DE performs superiorly to the others in this image. Also, it can be said that EVOA can also compete with ABC.

Table 4 shows the numerical results of the experiments conducted for the 4th image. When Table 4 is examined, GA produces the best results for the four-quality metrics for the 4th image. It produces the best results in two quality metrics, DE and EVOA. ABC, on the other hand, produces the best result for a quality metric. It can be said that GA performs better than the others for this image. Also, it can be said that DE and EVOA perform equally well.

Table 3. Experimental results for Image 3

	QM_{Var}	QM_{E}	QM_{SF}	QM_{SD}	QM_{ABF}	QM_{CB}	QM_{MI}	QM_{SCD}
				GA				
Max	4796,5094	7,7837	2,3946	69,2568	0,6968	0,7704	0,9297	0,1626
Mean	4791,8393	7,7421	2,3402	68,9532	0,6921	0,7660	0,9242	0,1573
SD	2,9967	0,0315	0,0304	0,2574	0,0031	0,0031	0,0028	0,0035
				DE				
Max	**4847,6539**	7,7788	**2,4482**	**69,6251**	**0,7112**	**0,7790**	0,9297	**0,2141**
Mean	4842,7669	7,7243	2,4051	69,0841	0,7069	0,7737	0,9251	0,2096
SD	3,4452	0,0271	0,0297	0,2590	0,0036	0,0033	0,0033	0,0033
				ABC				
Max	4822,3318	**7,7839**	2,4096	69,4430	0,6993	0,7746	0,9296	0,1868
Mean	4818,0853	7,7436	2,3638	68,9429	0,6944	0,7690	0,9244	0,1814
SD	2,5065	0,0271	0,0326	0,3278	0,0028	0,0031	0,0033	0,0034
				EVOA				
Max	4831,1246	7,7812	2,4191	69,5062	0,7069	0,7742	**0,9300**	0,1945
Mean	4825,9793	7,7312	2,3778	69,0992	0,7013	0,7696	0,9250	0,1900
SD	3,2322	0,0279	0,0296	0,2586	0,0034	0,0031	0,0036	0,0035

Boldfaced values indicate the "best" performances.

Table 4. Experimental results for Image 4

	QM_{Var}	QM_E	QM_{SF}	QM_{SD}	QM_{ABF}	QM_{CB}	QM_{MI}	QM_{SCD}
				GA				
Max	**3895,2398**	7,6520	4,3443	**62,4118**	**0,7365**	**0,7876**	0,8946	0,3913
Mean	3891,2508	7,6083	4,3000	61,8875	0,7314	0,7834	0,8906	0,3865
SD	3,4083	0,0309	0,0280	0,3245	0,0036	0,0031	0,0032	0,0035
				DE				
Max	3894,1864	**7,6525**	4,3472	62,4034	0,7364	0,7874	0,8946	**0,3923**
Mean	3888,9185	7,5978	4,3040	61,8967	0,7315	0,7826	0,8898	0,3870
SD	3,2738	0,0300	0,0327	0,2882	0,0037	0,0032	0,0033	0,0030
				ABC				
Max	3893,0045	7,6524	4,3484	62,3939	0,7354	0,7874	0,8949	0,3903
Mean	3888,0230	7,5997	4,3049	61,9339	0,7297	0,7826	0,8898	0,3861
SD	3,1932	0,0298	0,0328	0,3137	0,0034	0,0035	0,0027	0,0030
				EVOA				
Max	3890,6701	7,6522	**4,3539**	62,3752	0,7365	0,7873	**0,8949**	0,3892
Mean	3885,7726	7,6043	4,2940	61,8454	0,7317	0,7823	0,8897	0,3847
SD	3,1889	0,0319	0,0320	0,3215	0,0033	0,0033	0,0029	0,0034

Boldfaced values indicate the "best" performances.

When Table 1-4 is generally examined, it can be said that the optimization algorithms compared based on quality metrics give similar results. It can be said that DE and ABC produce the best results regarding more quality metrics. Thus, it can be said that DE and ABC give similar results, and GA and EVOA give similar results.

Figure 4-7 shows the fused images obtained within the scope of the experiments carried out for the images and the zoom images of these images. The first row for each image shows the fused images obtained with GA, DE, ABC, and EVOA, respectively. In the second line, the zoom of the fused images is respectively demonstrated, to make a subjective evaluation.

Figure 4 shows the fused images obtained for image 1. As shown in Figure 4, when the zoomed images are examined carefully, it is seen that ABC and EVOA give similar and better results than the other algorithms. When DE and GA are compared, it can be said that DE gives better results. In the numerical results in Table 1, DE and ABC gave better results than the others. Thus, it can be said that only numerical evaluation is insufficient and may give meaningless results in some cases.

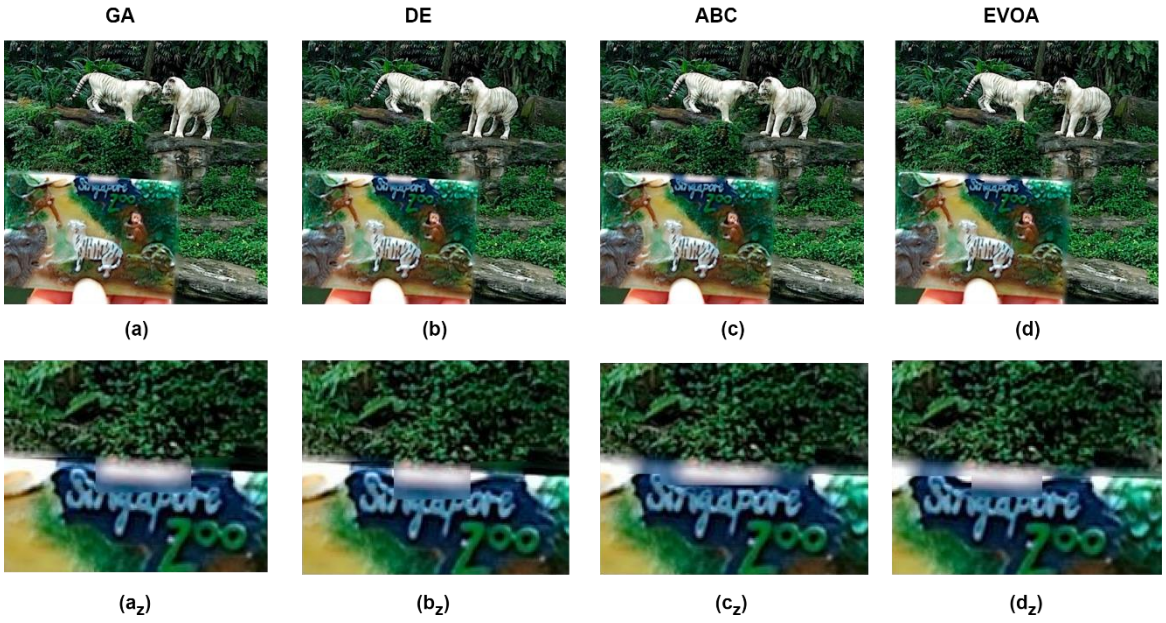

Figure 4. The obtained fused image for image 1

Figure 5. The obtained fused image for image 2

Figure 5 shows the fused images obtained for image 2. When Figure 5 is examined, it is seen that all optimization algorithms give similar results. In the numerical data of Table 2, the ABC algorithm achieves the best result based on seven quality metrics. However, there is no significant difference between the algorithms in subjective evaluation.

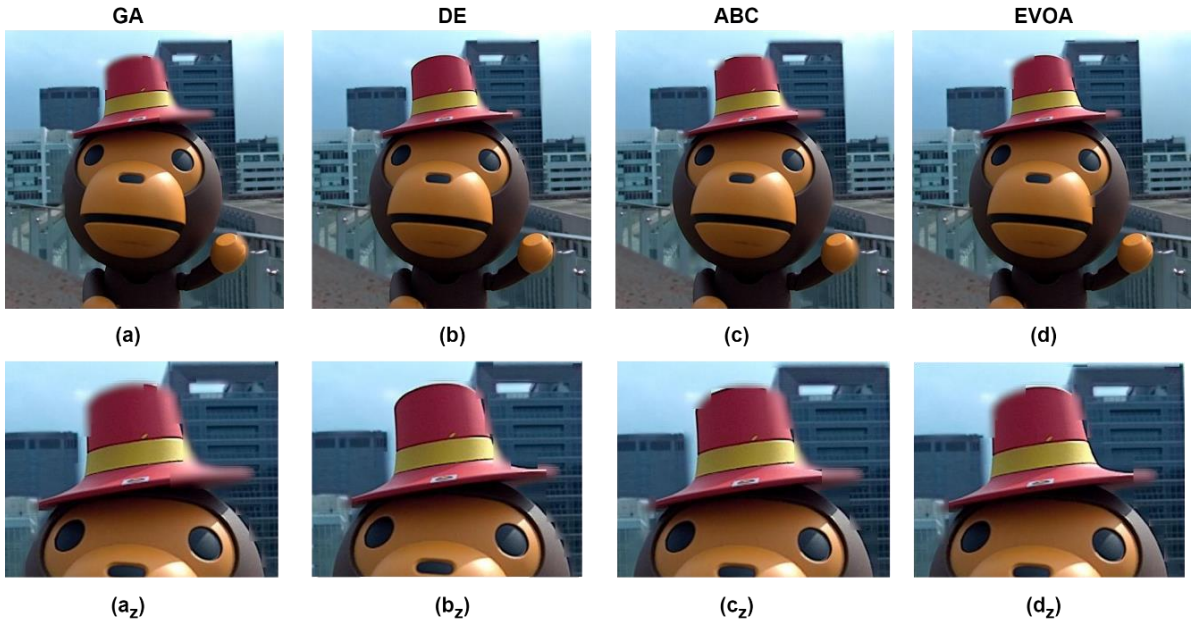

Figure 6. The obtained fused image for image 3

Figure 6 shows the fused images obtained for image 3. When Figure 6 is examined, it is obvious that the method's performance decreases and makes incorrect fusing in photographs containing non-linear objects. The main disadvantage of block-based multi-focus image fusion methods is seen in Figure 6. As seen in Figure 6, DE gives better results than the others. Then, while ABC and EVOA obtain similar results, it is seen that GA performs the worst fusing process. When evaluated together with the numerical results obtained in Table 3 for this image, it is seen that a result equivalent to the subjective evaluation is reached.

Figure 7. The obtained fused image for image 4

Figure 7 shows the fused images obtained for image 4. When Figure 7 is examined, although the image has non-linear objects, the optimization algorithms obtained well-fused images close to each other. When Figure 4-7 is generally reviewed, it is seen that the algorithms give similar results and can compete with each other.

4. Conclusion

This work proposes using the recently proposed energy valley optimization algorithm (EVOA) for multi-focus image fusion. Multi-focus image fusion is the method of obtaining a clear image on all sides by combining multi-focus images of the same scene. These fused images are widely used in many fields, from the military to the medical field. EVOA is a new meta-heuristic optimization algorithm presented by Azizi et al. in 2023. EVOA is used to calculate optimal block sizes. The method is applied to commonly used image sets. Despite the development of numerous quality assessment metrics in the literature, evaluating fused images remains challenging. While one quality metric may yield favorable results for an image, another metric may produce less favorable outcomes for the same image. Thus, relying on a single quality metric may be insufficient for objective assessment.

Consequently, multiple quality metrics are employed for objective evaluation. In addition to objective assessment, conducting subjective evaluations is also crucial. Both objective and subjective evaluations are made to evaluate the quality of the resulting fused images. When the results are compared with the well-known GA, DE and ABC, it was seen that EVOA showed a performance close to the others.

In this study, EVOA is used to optimize the block size. By changing the parameter values of EVOA, experiments can be conducted, and the results compared. Experiments can be run using different current meta-heuristic optimization algorithms, and the results can be compared. Optimized block-based image fusion is used in this study. Other optimization algorithms can be used for region-based multi-focus image fusion methods and the performance of these algorithms can be evaluated.

Author Contributions

The author read and approved the final version of the paper.

Conflicts of Interest

The author declares no conflict of interest.

Ethical Review and Approval

No approval from the Board of Ethics is required.

References

[1] V. Aslantas, R. Kurban, *Fusion of multi-focus images using differential evolution algorithm*, Expert Systems with Applications 37 (12) (2010) 8861–8870.

[2] C. Akyel, *Diagnosis of oral cancer from histopathological images with xception*, Journal of Advanced Research in Natural and Applied Sciences 9 (2) (2023) 283–290.

[3] H. Avcı, J. Karakaya, *Effect of different parameter values for pre-processing of using mammography images*, Journal of Advanced Research in Natural and Applied Sciences 9 (2) (2023) 345–354.

[4] F. Çakıroğlu, R. Kurban, A. Durmuş, E. Karaköse, *Multi-focus image fusion by using swarm and physics based metaheuristic algorithms: A comparative study with Archimedes, atomic orbital search, equilibrium, particle swarm, artificial bee colony and jellyfish search optimizers*, Multimedia Tools and Applications 82 (29) (2023) 44859–44883.

[5] G. Pajares, J. M. De La Cruz, *A wavelet-based image fusion tutorial*, Pattern Recognition 37 (9) (2004) 1855–1872.

[6] P. Burt, E. Adelson, *The Laplacian Pyramid as a compact image code*, IRE Transactions on Communications Systems 31 (4) (1983) 532–540.

[7] S. Li, B. Yang, *Multifocus image fusion by combining curvelet and wavelet transform*, Pattern Recognition Letters 29 (9) (2008) 1295–1301.

[8] M. N. Do, M. Vetterli, *The contourlet transform: An efficient directional multiresolution image representation*, IEEE Transactions on Image Processing 14 (12) (2005) 2091–2106.

[9] Q.-G. Miao, C. Shi, P.-F. Xu, M. Yang, Y.-B. Shi, *A novel algorithm of image fusion using shearlets*, Optics Communications 284 (6) (2011) 1540–1547.

[10] M. Nejati, S. Samavi, S. Shirani, *Multi-focus image fusion using dictionary-based sparse representation*, Information Fusion 25 (2015) 72–84.

[11] M. Nejati, S. Samavi, N. Karimi, S. M. R. Soroushmehr, S. Shirani, I. Roosta, K. Najarian, *Surface area-based focus criterion for multi-focus image fusion*, Information Fusion 36 (2017) 284–295.

[12] S. Bhat, D. Koundal, *Multi-focus image fusion techniques: A survey*, Artificial Intelligence Review 54 (8) (2021) 5735–5787.

[13] S. Li, J. T. Kwok, Y. Wang, *Combination of images with diverse focuses using the spatial frequency*, Information Fusion 2 (3) (2001) 169–176.

[14] Y. Chen, J. Guan, W.-K. Cham, *Robust Multi-Focus image fusion using Edge model and Multi-Matting*, IEEE Transactions on Image Processing 27 (3) (2018) 1526–1541.

[15] A. N. Toprak, V. Aslantas, *Fusion of multi-focus image by blocks optimal positions*, in: E. Adalı, Ş. Sağıroğlu (Eds.), 3rd International Conference on Computer Science and Engineering (UBMK), Sarayova, 2018, pp. 471–476.

[16] V. Aslantas, A. N. Toprak, *Multi focus image fusion by differential evolution algorithm*, in: J. Filipe, O.

Gusikhin (Eds), 11th International Conference on Informatics in Control, Automation and Robotics (ICINCO), Vienna, 2014, pp. 312–317.

[17] J. Kong, K. Zheng, J. Zhang, X. Feng, *Multi-focus image fusion using spatial frequency and genetic algorithm*, International Journal of Computer Science and Network Security 8 (2) (2008) 220–224.

[18] R. Özdemir, M. Taşyürek, V. Aslantaş, *Improved Marine Predators Algorithm and Extreme Gradient Boosting (XGBoost) for shipment status time prediction*, Knowledge-Based Systems 294 (2024) 111775 20 pages.

[19] M. Taşyürek, M. Erat, *Determining the best meter reading route using ant colony and genetic algorithm methods*, Dicle University Journal of Engineering 13 (3) (2022) 405–412.

[20] M. Azizi, U. Aickelin, H. A. Khorshidi, M. B. Shishehgarkhaneh, *Energy valley optimizer: A novel metaheuristic algorithm for global and engineering optimization*, Scientific Reports 13 (1) (2023) Article Number 226 23 pages.

[21] M. Eskicioglu, P. S. Fisher, *Image quality measures and their performance*, IEEE Transactions on Communications 43 (12) (1995) 2959–2965.

[22] V. Aslantas, R. Kurban, *A comparison of criterion functions for fusion of multi-focus noisy images*, Optics Communications 282 (16) (2009) 3231–3242.

[23] J. H. Holland, An introductory analysis with applications to biology, control and artificial intelligence, Adaptation in Natural and Artificial System, MIT Press, Cambridge, 1992, Ch. 1-14, 211 pages.

[24] R. Storn, K. Price, *Differential evolution - A simple and efficient heuristic for global optimization over continuous spaces*, Journal of Global Optimization 11 (4) (1997) 341–359.

[25] D. Karaboga, B. Basturk, *A powerful and efficient algorithm for numerical function optimization: Artificial bee colony (ABC) algorithm*, Journal of Global Optimization 39 (3) (2007) 459–471.

[26] K. Ma, N. K. Zeng, N. Z. Wang, *Perceptual quality assessment for multi-exposure image fusion*, IEEE Transactions on Image Processing 24 (11) (2015) 3345–3356.

[27] Y. Liu, S. Liu, Z. Wang, A *general framework for image fusion based on multi-scale transform and sparse representation*, Information Fusion 24 (2015) 147–164.

[28] C. S. Xydeas, V. Petrovic, *Objective image fusion performance measure*, Electronics Letters 36 (4) (2000) 308 3 pages.

[29] Y. Chen, R. S. Blum, *A new automated quality assessment algorithm for image fusion*, Image and Vision Computing 27 (10) (2009) 1421–1432.

[30] B. Wei, X. Feng, K. Wang, B. Gao, *The Multi-Focus-Image-Fusion method based on convolutional neural network and sparse representation*, Entropy 23 (7) (2021) 827 16 pages.

[31] V. Aslantas, E. Bendes, *A new image quality metric for image fusion: The sum of the correlations of differences*, AEÜ. International Journal of Electronics and Communications 69 (12) (2015) 1890–1896.